

Tribology International 32 (1999) 71-81



www.elsevier.com/locate/triboint

# Simulating sliding wear with finite element method

Priit Põdra a,\*, Sören Andersson b

<sup>a</sup> Department of Machine Science, Tallinn Technical University, TTU, Ehitajate tee 5, 19086 Tallinn, Estonia <sup>b</sup> Machine Elements, Department of Machine Design, Royal Institute of Technology, KTH, S-100 44 Stockholm, Sweden

Received 5 September 1997; received in revised form 18 January 1999; accepted 25 March 1999

## Abstract

Wear of components is often a critical factor influencing the product service life. Wear prediction is therefore an important part of engineering. The wear simulation approach with commercial finite element (FE) software ANSYS is presented in this paper. A modelling and simulation procedure is proposed and used with the linear wear law and the Euler integration scheme. Good care, however, must be taken to assure model validity and numerical solution convergence. A spherical pin-on-disc unlubricated steel contact was analysed both experimentally and with FEM, and the Lim and Ashby wear map was used to identify the wear mechanism. It was shown that the FEA wear simulation results of a given geometry and loading can be treated on the basis of wear coefficient—sliding distance change equivalence. The finite element software ANSYS is well suited for the solving of contact problems as well as the wear simulation. The actual scatter of the wear coefficient being within the limits of ±40–60% led to considerable deviation of wear simulation results. These results must therefore be evaluated on a relative scale to compare different design options. © 1999 Elsevier Science Ltd. All rights reserved.

Keywords: Wear simulation; FEA; Wear tests; Contact temperature

#### 1. Introduction

The most confident knowledge about the friction pair tribological behaviour can be achieved by making wear experiments. However, the particular design alternatives need to be evaluated quickly on a regular in-house routine basis. A massive amount of research has been carried out to help designers with that respect.

It has been argued that the dominating parameters contributing to the sliding wear of a given system are the loading and the relative sliding of the contact. The velocity is determined by the mechanism kinematics. The question of how the system load influences the actual contact stress field is more complicated. The first relevant analysis of the stress at the contact of two elastic solids was presented by Hertz. He regarded the contacting bodies as elastic half-spaces and the contact between them ellipse-shaped, frictionless and non-con-

Wear takes place when surfaces of mechanical components contact each other. The question of great practical importance is, how much of the material will be lost during the given operation time. The surface shapes vary due to their functions, manufacturing tolerances, etc. and will be changed as a result of wear and plastic deformation. The pressure distribution is then strongly dependent on those phenomena. A finite element method (FEM) is a versatile tool to solve the stress and strain problems regardless of the geometry of the bodies. A FEA program ANSYS 5.0A has been used in this paper for the contact pressure determination as well as wear simulation.

## 2. Wear models

The wear process can be treated as a dynamic process, depending on many parameters and the prediction of that process as an initial value problem. The wear rate may then be described by a general equation

forming. This approach has often been used in the contact stress calculations.

<sup>\*</sup> Corresponding author. Tel.: +372-620-33-02; fax: +372-620-31-96.

E-mail addresses: priitp@edu.ttu.ee (P. Põdra), soren@damek.kth.se (S. Andersson)

#### **Nomenclature**

apparent contact area (m2)  $\boldsymbol{A}$ thermal diffusivity (m<sup>2</sup>/s)  $a_0$ D stiffness (N/m) Eelastic modulus (Pa)  $E^*$ normalised elastic modulus (Pa)  $f_{\rm Fr}$ friction coefficient load (N)  $F_{N}$ normal load (N) Hhardness (Pa) HVVickers hardness (Pa)

h wear depth (m)

dimensional wear coefficient (Pa<sup>-1</sup>) k

K wear coefficient

 $K_{\rm m}$ thermal conductivity of steel (J/m/s/K)

KNcontact stiffness (N/m) Mtime scale factor

normal contact pressure (Pa) p  $\tilde{p}$ dimensionless normalised pressure

PePéclet number q'' $\tilde{Q}$ heat flux (W/m<sup>2</sup>)

dimensionless normalised wear rate apparent contact area radius (m)  $r_0$  $\frac{r_{\rm p}}{R}$ pin sliding track average radius (m)

pin tip radius (m)

 $R_1$ torus profile radius of curvature (m)

S sliding distance (m)

time (s) t

Ttemperature (K)

Nodal displacement (m) и

velocity (m/s)  $\nu$ 

ũ dimensionless normalised velocity

Vvolume wear (m<sup>3</sup>)

Cartesian coordinates (m) x, y

 $\alpha$ cone angle (°)

heat distribution coefficient  $\alpha_{12}$ 

difference, increment  $\Delta$ spinning angle (rad)

Poisson ratio μ

## Subscripts

aver average

Contact belongs to contact Disc belongs to disc flash flash temperature

sampling point encounter

in initial

solution step encounter lim maximum allowed

max maximum Pin belongs to pin  $\frac{dh}{ds} = f$  (load, velocity, temperature,

material parameters, lubrication, . . . )

where h is the wear depth (m) and s is the sliding distance (m). Many wear models are available in the literature. Their mathematical expressions vary from simple empirical relationships to complicated equations relying on physical concepts and definitions [1]. Specific parameters and variables are often involved, valid only for a particular case and not available in handbooks. Therefore very few of those models have been used to predict wear in practice.

A comprehensive wear classification for steels over the wide range of loads and sliding velocities was given by Lim and Ashby [2]. They based their work on simplified wear equations and adjusted them on the basis of data from a large number of dry pin-on-disc experiments. This work resulted in a wear map, Fig. 1, giving the contours of wear regimes and the dimensionless wear rate  $\tilde{Q}$  as a function of dimensionless normalised pressure  $\tilde{p}$  and dimensionless normalised velocity  $\tilde{v}$ , defined

$$\tilde{Q} = \frac{V}{As}$$
,  $\tilde{p} = \frac{F_{\rm N}}{AH}$  and  $\tilde{v} = \frac{vr_0}{a_0}$  (1)

where V is the volume wear ( $m^3$ ), A is the apparent contact area (m<sup>2</sup>) and  $r_0$  is its radius (m),  $F_N$  is the normal load (N), H is the hardness (Pa) of softer material in contact, v is the relative sliding velocity (m/s) and  $a_0$  is the material's thermal diffusivity (m<sup>2</sup>/s). The wear equations and the parameters used by Lim and Ashby are shown in Table 1.

The temperature analysis, on which the wear map in Fig. 1 was based assumed a simple 1-dimensional heat flow. Further, in the regime in which the flash temperatures play an important role on wear, the heat distribution coefficient was taken to be equal to  $\alpha_{12}$ =0.5. If the contact flash temperature is above 700°C, the oxidational wear mechanism will prevail in a steel contact. Below this temperature limit, the wear law was proven to be linear with respect to load and independent of velocity.

The most frequently used model is the linear wear equation  $\tilde{Q}=K\tilde{p}$ , where the volume wear rate is proportional to the normal load. This model is often referred to as the Archard's wear law, though its basic form was first published by Holm [3]. The model was based on experimental observations and written in the form

$$\frac{V}{s} = K \frac{F_{\rm N}}{H} \tag{2}$$

The wear coefficient K was introduced to provide agreement between theory and experiment. Holm treated it as a constant, representing the number of abraded

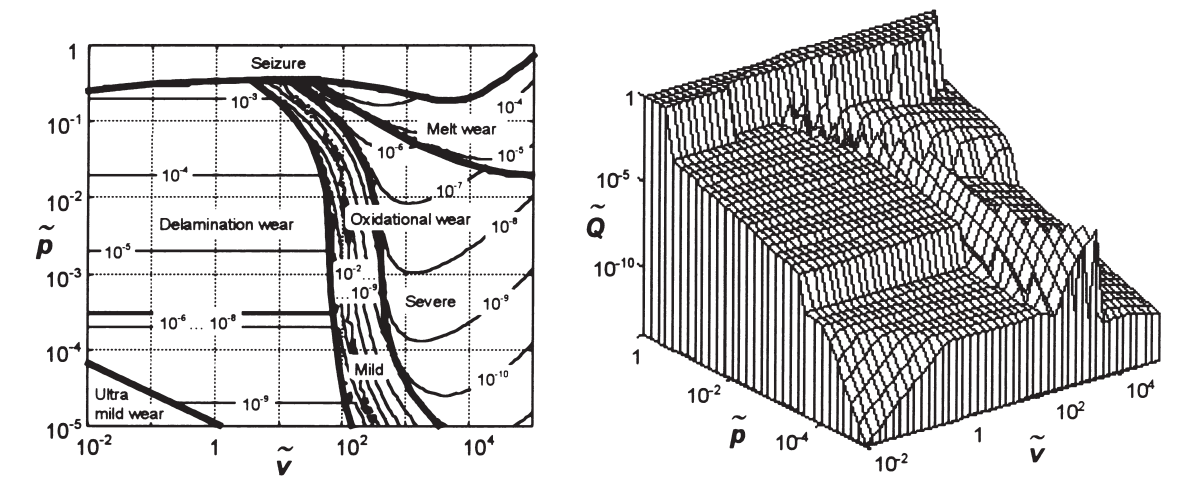


Fig. 1. Lim and Ashby wear map and its 3-dimensional plot.

atoms per atomic encounter. In Archard's work it corresponds to the probability that an asperity interaction results in a wear particle formation [4]. However, that is not the only possible interpretation. Lim and Ashby [2] calculated it regarding the delamination or plasticity dominated wear mechanism as governing. For steels they suggested to use the values

$$\begin{cases} K = 5.10^{-5} & \text{if } \tilde{p} < 3.10^{-4} \\ K = 5.10^{-3} & \text{if } \tilde{p} > 3.10^{-4} \end{cases}$$

However, the actual value of K for a particular contact should normally be experimentally determined and is always less than unity.

For engineering applications the wear depth is of more interest, than wear volume. Here Archard proposed to divide both sides of Eq. (2) by the apparent contact area A [4], giving

$$\frac{V}{sA} = \frac{h}{s} = kp$$

where h is the wear depth (m), k is the dimensional wear coefficient (Pa<sup>-1</sup>) and p is the normal contact pressure (Pa). The wear process can be regarded as a dynamic process and its prediction an initial value problem. The wear model can then be described by a differential equation, which for the linear case, Eq. (2) can be formulated as

$$\frac{\mathrm{d}h}{\mathrm{d}s} = kp \tag{3}$$

## 3. FEA wear simulation procedure

## 3.1. Finite element theory

The main task of the finite element method (FEM) in the wear calculations is to compute the fields of contact stresses. The structure to be analysed is discretised with a number of elements, assembled at nodes. In FEM the function in question (displacement, temperature, etc.) is piecewise approximated by means of polynomials over every element and expressed in terms of nodal values [5]. The elements of different type and shape with complex loads and boundary conditions can be used simultaneously. In the structural analysis the degrees of freedom are defined as nodal displacements. The equations for every element are assembled into a set, expressed in the structural level as

$$[D]{u} = {F}$$

where [D] is the structural or global stiffness (N/m) matrix,  $\{u\}$  is the structural nodal displacement or deformation (m) vector and  $\{F\}$  is the vector of structural nodal loads (N). This equation system can be solved for  $\{u\}$ . From deformations the nodal stresses are computed. The commercial finite element (FE) software ANSYS can handle several material and structural non-linearities, such as plasticity, viscoelasticity, friction, etc., [6]. The coupled-field analyses, for instance thermal–structural, can be performed as well.

The FE wear calculations involve solving the general contact problem with the area of contact between the bodies not known in advance. The analysis is therefore non-linear. The point-to-surface interface elements are used in those cases. FEA software is equipped with many tools, enhancing the non-linear numerical procedure, the parameters of which are to be chosen with care.

## 3.2. Wear simulation routine

The flow-chart of the FE wear simulation procedure, consisting of a series of structural solution steps combined with additional calculations, is shown in Fig. 2.

The initial parameters given define the model geometry, loads, constraints and wear model parameters

Table 1 Wear models and parameters used by Lim and Ashby [2]

	_		
Seizure:	$\tilde{p}_{\text{seizure}} = \frac{1}{\sqrt{1 + \alpha_t f_{\text{Fr}}^2}} \left( 1 - \frac{T_{\text{bulk}} - T_0}{20 T_{\text{melt}}} \ln \frac{10^6}{\beta \tilde{v}} \right)$	(the real contact area equa	als the apparent contact area: <i>N</i> =1)
Melt wear:	$\tilde{Q}_{\text{melt}} = \frac{(T_{\text{melt}} - T_0)H}{T^* L_{\text{melt}} \beta \tilde{v}} \left( \alpha_{12} f_{\text{Fr}} \tilde{p} \tilde{v} \frac{T^* \beta}{T_{\text{melt}} - T_0} - 1 \right)$	(the surface bulk temperature equals the melting point $T_{\rm melt}$ )	
Mild-oxidational wear:	$\tilde{Q}_{\text{mild-ox}} = \frac{C_0^2 A_0 r_0 \tilde{p}}{Z_C a_0 \tilde{v}} \exp\left(-\frac{E_0}{R_0 T_{\text{flash}}}\right)$	(the flash temperatures are above 700°C)	
Severe-oxidational wear:	$\tilde{Q}_{\text{sev-ox}} = \int_{\text{m}} \frac{K_{\text{ox}}(T_{\text{melt-ox}} - T_{\text{bulk}}) \sqrt{\tilde{p}N}}{L_{\text{melt,ox}} a_0 \beta \tilde{v}} \left[ \frac{\alpha_{12} f_{\text{Fr}} H \beta \tilde{v}}{K_{\text{ox}}(T_{\text{melt,ox}} - T_{\text{bulk}})} \sqrt{\frac{\tilde{p}}{N}} - 1 \right]$		
Delamination wear:	$ ilde{Q}_{ m delamin} = \! K  ilde{p}$	J	
$\alpha_{12} = \frac{1}{2 + \beta \sqrt{\pi \vec{v}/8}}$	heat distribution coefficient between bodies 1 and 2	$\beta = \frac{l_{\text{bulk}}}{r_0} = 6$	dimensionless number
$N = \left(\frac{r_0}{r_a}\right)^2 \tilde{p}(1-\tilde{p}) + 1$	number of contacting asperities	$C_0 = \frac{3M_{\rm Fe}}{2M_{\rm O_2}\rho_{\rm Fe}} = 3.4 \cdot 10^{-6}$	constant (m³/kg)
$T_{\mathrm{bulk}} = T_0 + f_{\mathrm{Fr}} T^* \beta \tilde{p} \tilde{v}$	bulk temperature (K)	$f_{\rm Fr} = 0.78 - 0.13 \log(\tilde{v})$	friction coefficient
$T_{\mathrm{flash}} = T_{\mathrm{bulk}} + \frac{1}{2} f_{\mathrm{Fr}} T_{\mathrm{C}}^* \beta \tilde{v} \sqrt{\frac{\tilde{p}}{N}}$	flash temperature (K)	$K = \frac{2\gamma_0 f_{\rm V}}{f_{\rm A}^*} = 4.10^{-5}$	wear coefficient for steel
$T^* = \frac{a_0 H}{K_{\rm m}} = 222$	equivalent temperature for steel (K)	$T_{\rm C}^* = \frac{aH}{K_{\rm C}} = 650$	effective equivalent temperature for steel (K)
$a_0 = 9.1 \cdot 10^{-6}$	thermal diffusivity of steel (m²/s)	$l_{\rm bulk} = 9 \cdot 10^{-3}$	equivalent linear diffusion distance for bulk
$A_0=10^6$ $\alpha_t=12$ $E_0=1.38\cdot10^5$ $f^*_A=0.5$ $f_m=0.01$	Arrhenius constant for oxidation (kg²/m⁴/s) constant activation energy for oxidation (J/mol) critical area fraction of voids volume fraction of the removed molten material	$L_{\text{melt},ox} = 2.1 \cdot 10^{9}$ $L_{\text{melt},ox} = 3.1 \cdot 10^{9}$ $M_{\text{Fe}} = 56$ $M_{\text{O}_2} = 32$ $r_0 = 1.5 \cdot 10^{-3}$	heating (m) latent heat of steel melting (J/m³) latent heat of oxide melting (J/m³) molecular weight of iron molecular weight of oxygen radius of contact area (m)
$f_{\rm V}=10^{-3}$ $\gamma_0=0.01$	volume fraction of inclusions plastic shear strain ratio per pass	$r_{\rm a}$ =10 <sup>-5</sup> $R_0$ =8.314 $\rho_{\rm Fe}$ =7800	asperity tip radius (m) molar gas constant (J/mol/K) density of steel (kg/m³)
$H=10^9$ $K_{\rm C}=14$ $K_{\rm m}=41$ $K_{\rm ox}=3.2$	hardness of steel (Pa) effective thermal conductivity (J/m/s/K) thermal conductivity of steel (J/m/s/K) thermal conductivity of oxide (J/m/s/K)	$T_0$ =300 $T_{\text{melt}}$ =1800 $T_{\text{melt,ox}}$ =1867 $Z_{\text{C}}$ =10 <sup>-5</sup>	sink temperature (K) melting point for steel (K) melting point for oxide (K) critical oxide film thickness (m)

along with the element and material data. Special subroutines were developed for every configuration to generate the FE model and define the loads and constraints automatically.

A good discretisation must be found for every particular geometry and loading case. The areas with expected high stress gradients utilise a finer node mesh. More elements in the model are likely to provide more exact results, but contribute to an increased computing time and use of disk space.

After the FEA iterative stress solution was obtained,

the contact region was located. The status of every contact element (closed or not) was determined. The contact node coordinates of closed contact elements define the contact area location. The nodal stresses of the nodes in the contact region determine the contact pressure distribution.

The Euler method is used to integrate the wear law with respect to time. For each wear simulation step the system parameters are assumed to be constant and contributing to the wear depth at every node according to the following discretised wear model

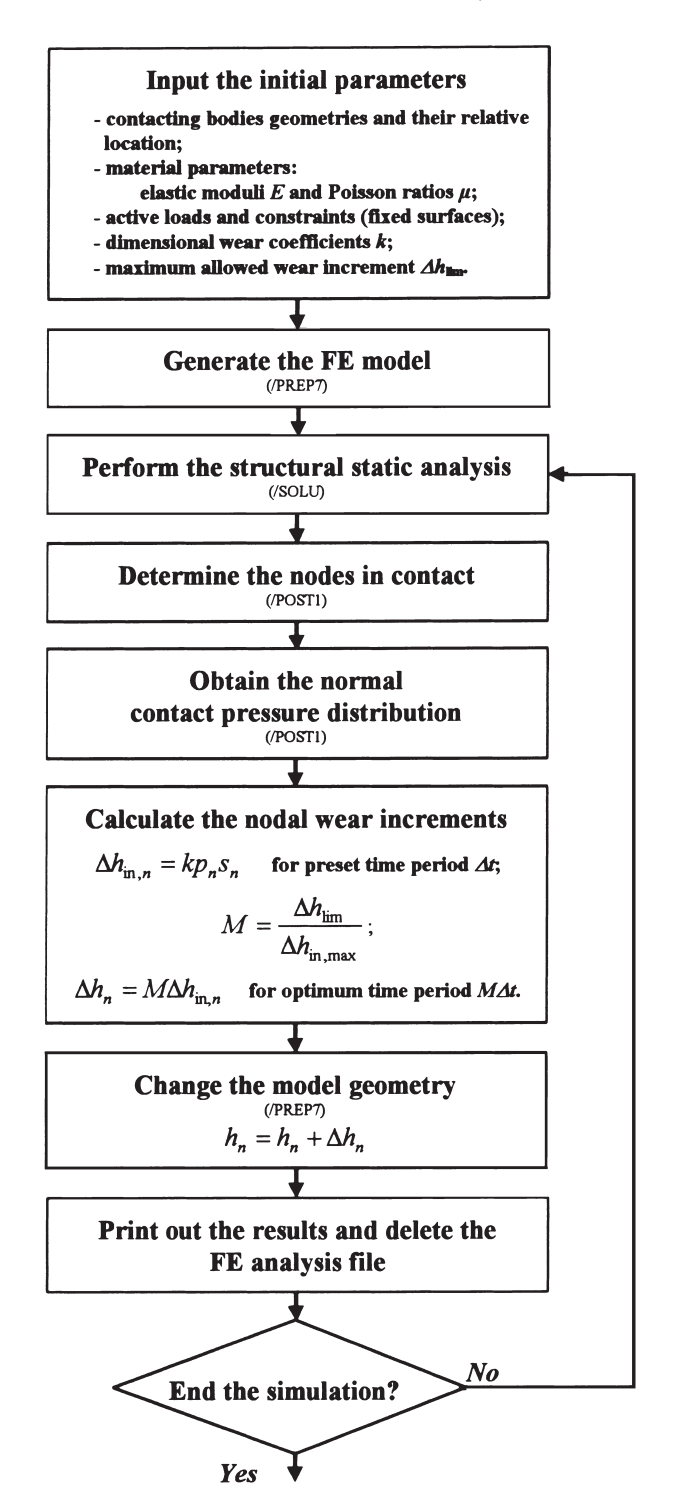


Fig. 2. FE wear simulation approach.

$$h_{i,n} = h_{i-1,n} + \Delta h_{i,n} \tag{4}$$

where  $\Delta h_{j,n}$  is the wear increment (m) at node n and j is the solution step encounter. With the stress distribution known, the nodal wear increments  $\Delta h_{j,n}$  (m) were evaluated. The simulation results might however become erratic, if the difference between the nodal wear increments of one simulation step is too large. An unex-

pected gap could appear between the bodies in the contact area. A maximum allowed wear increment  $\Delta h_{\rm lim}$  (m) was therefore introduced and predefined for each model geometry and loading case on the basis of experience. Short simulation test runs were made to adjust its value to be as large as possible.

First the initial nodal wear increments  $\Delta h_{\text{in},j,n}$  (m) were computed for a constant time increment  $\Delta t$  (s). The time scale factor  $M_j$  for every solution step j was then evaluated as

$$M_j = \frac{\Delta h_{\text{lim}}}{\Delta h_{\text{in},i,\text{max}}}$$

where  $\Delta h_{\text{in,j,max}}$  is the maximum value (m) among the nodal wear increments  $\Delta h_{\text{in,j,n}}$ . The actual time interval for that step j will then be set equal to  $M_j\Delta t$ . The model geometry is thereafter changed by moving the nodes in contact into the new locations according to Eq. (4) with  $\Delta h_{j,n} = M_j \Delta h_{\text{in,j,n}}$ . This approach, instead of the use of constant time step, improved FEA running and speeded up the analysis. It was considered important to store a selected output data set into a special file after every solution step. This enabled quick data reviews afterwards and saved the previous steps' data, if the analysis had to be interrupted for some reason.

#### 3.3. FEA results verification

Perhaps the most convincing way to verify the FEA results is to compare them with the known analytical solutions. ANSYS software is also equipped with the energy error estimation technique, based on the fact that the FEA structural analysis results in a continuous displacement field from element to element, but a discontinuous stress field [6]. To obtain more acceptable stresses, the element nodal stresses are averaged. The nodal stress error vectors are accordingly evaluated, being a base for the energy error estimation for elements and over the entire model. When the energy errors are equal for every element, then that particular model with its given discretisation is the most efficient one.

#### 3.4. Sphere-on-plane FE model

The wear of the pin-on-disc configuration, Fig. 3, was analysed with the FEA approach outlined above. The plastic deformations and the influence of friction on the contact pressure distribution were considered to be negligible in this case. The structure with a spherical-ended pin with a radius of *R*=5 mm was thus represented in FEM by an axi-symmetrical sphere-on-plane contact model. Two-dimensional structural solid elements, designated as PLANE42 in ANSYS, were used for the solid parts of the model. The contact surfaces were modelled by two-dimensional point-to-surface contact

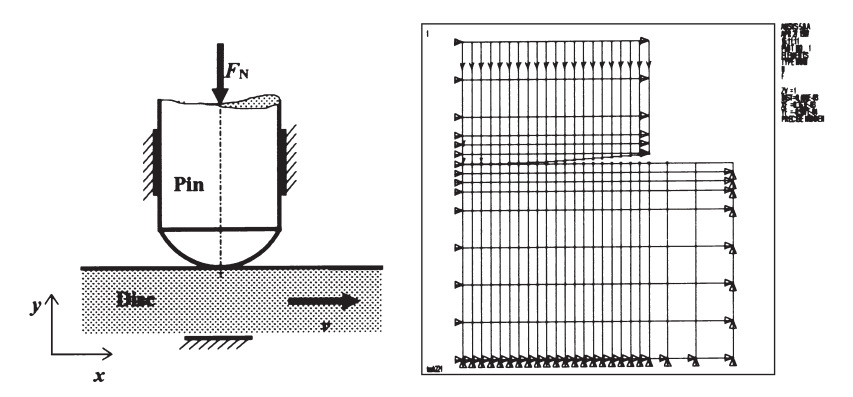


Fig. 3. Pin-on-disc rubbing contact and the FE model structure.

elements CONTAC48. Both the pin and the disc were considered to be made of steel with elastic moduli and Poisson ratios E=210 GPa and  $\mu$ =0.3 respectively. The two normal loads were  $F_N$ =21 N and  $F_N$ =50 N. The x-directional size of the contact region element was 25  $\mu$ m and 32.5  $\mu$ m respectively, depending on the load. The corresponding y-directional lengths were 25  $\mu$ m and 42  $\mu$ m. The ANSYS contact stiffness parameter was set to KN=5·10 $^7$  N/m.

In order to check the model validity, the normal contact pressure distributions were calculated by both the FEA and the Hertz formulae for sphere-on-plane configuration (Fig. 4)

$$p = p_{\text{max}} \left( 1 - \frac{x^2}{r_0^2} \right) \text{ with } \begin{cases} r_0 = \sqrt[3]{\frac{3F_N R}{4E^*}} \\ p_{\text{max}} = \frac{3F_N}{2\pi r_0^2} \end{cases}$$

where  $E^*=E/2(1-\mu^2)$  is the normalised elasticity modulus (Pa). The plastic deformations were disabled and the friction was neglected in the model. The discrepancy between the FE numerical and Hertz analytical solutions did not exceed 5%.

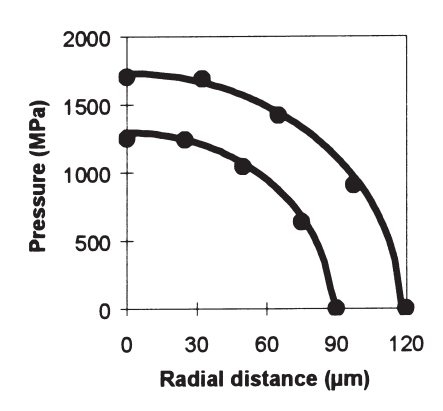


Fig. 4. Hertz (continuous line) and FEA (black dots) sphere-on-plane normal pressure distributions for steels with *R*=5 mm.

# 4. Experimental procedure

Unlubricated pin-on-disc experiments were made with a spherical steel pin with a radius of R=5 mm sliding on a steel disc with normal load  $F_N=21$  N or  $F_N=50$  N. The discs and the pins were hardened to HV=4.6 GPa and HV=3 GPa, respectively, thus the maximum contact pressures, calculated by Hertz, were assumed to be within the elastic limits (Fig. 4). The test rig allowed online measurement of the wear depth and friction torque (Fig. 5). The sliding velocity in the tests was v=25 mm/s.

The experimental results are shown in Fig. 6. Two tests at each load were done. The wear coefficients, Fig. 6(c), were determined from the average wear depths from both tests, Fig. 6(a), and by using the following equation

$$k_i = \frac{\Delta V_i}{\Delta s F_N}$$

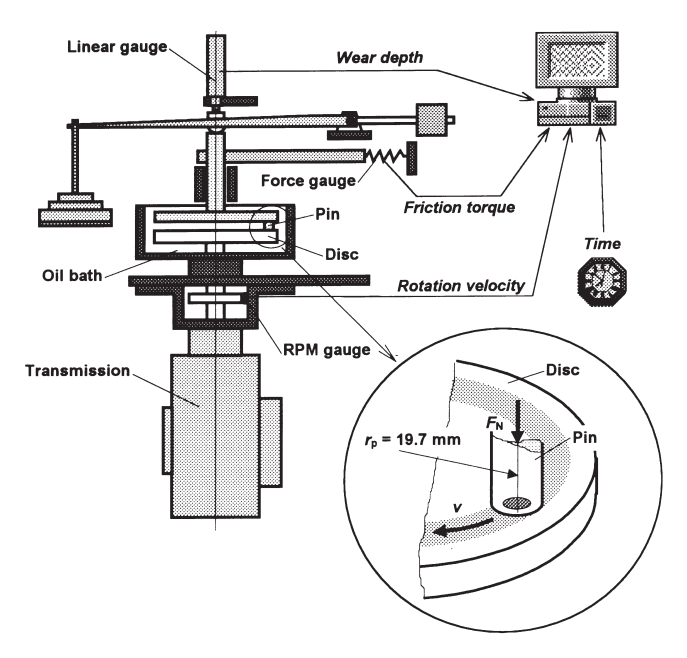


Fig. 5. Pin-on-disc test rig.

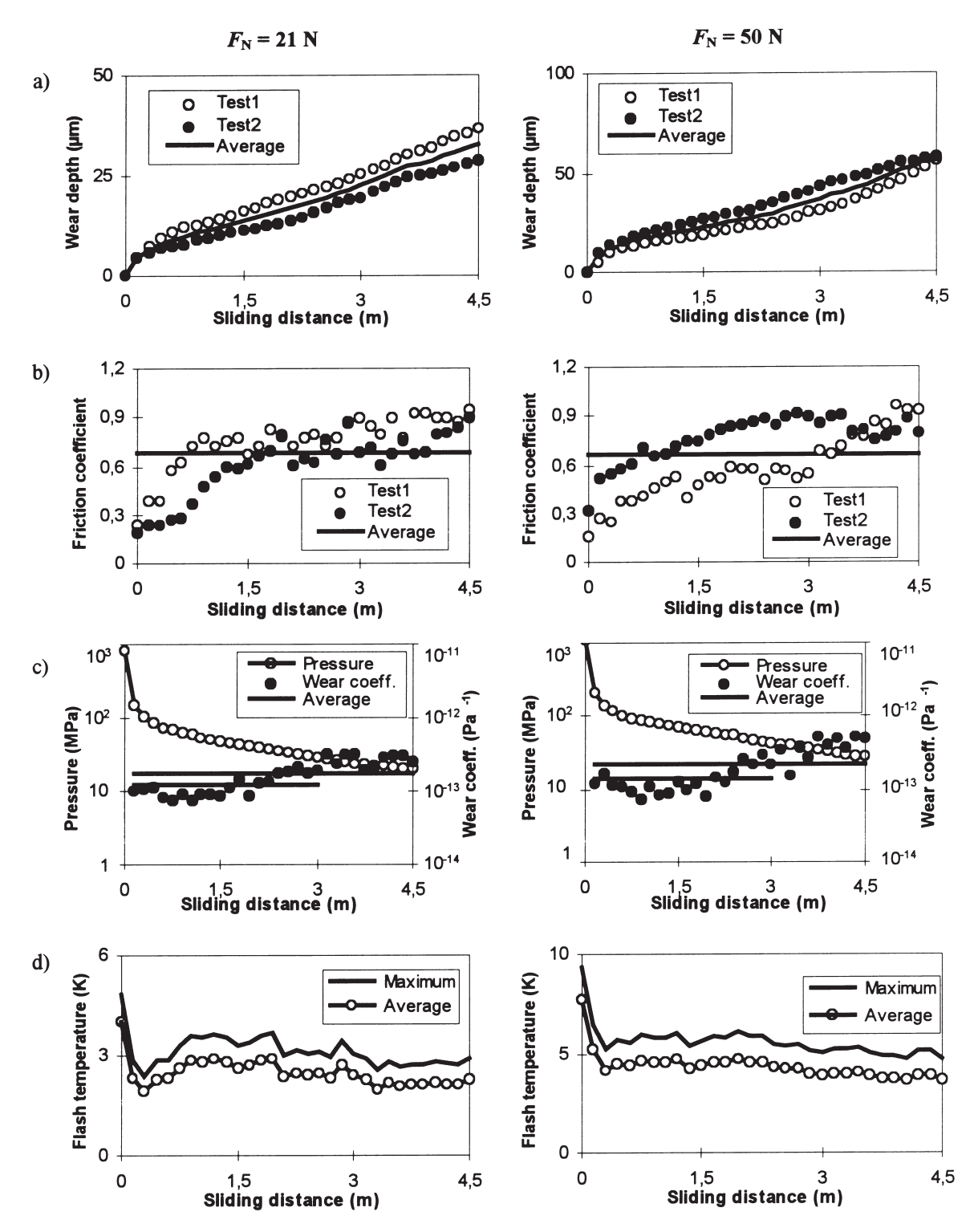


Fig. 6. Pin-on-disc experiment data for steels as a function of sliding distance: (a) pin wear depth; (b) friction coefficient; (c) normal contact pressure and wear coefficient; (d) contact flash temperatures.

where the volume wear increments were determined by the formula [7] (Fig. 7)

$$\Delta V_i = \frac{\pi}{3} [h_i^2 (3R - h_i) - h_{i-1}^2 (3R - h_{i-1})]$$

where  $i \ge 1$  is the sampling point number and  $\Delta s = 0.15$ 

m is the sliding distance increment. The discs were harder than pins and the wear test left no measurable prints on the disc surfaces. The average wear coefficients were evaluated from experiment data for sliding distances s=3 m and s=4.5 m [Fig. 6(c)]. These values with the standard deviation were  $k=(1.25\pm0.44)\cdot10^{-13}$  Pa<sup>-1</sup>

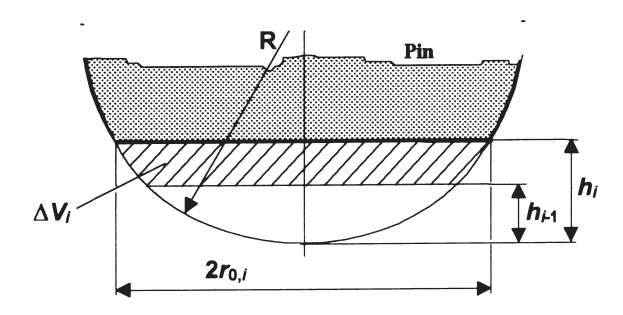


Fig. 7. Volume wear of pin.

and k=(1.76±0.85)·10<sup>-13</sup> Pa<sup>-1</sup> in tests with  $F_N$ =21 N and k=(1.42±0.62)·10<sup>-13</sup> Pa<sup>-1</sup> and k=(2.26±1.44)·10<sup>-13</sup> Pa<sup>-1</sup> with  $F_N$ =50 N. The overall average wear coefficients were computed from both test series as k=(1.33±0.54)·10<sup>-13</sup> Pa<sup>-1</sup> and k=(2.01±1.21)·10<sup>-13</sup> Pa<sup>-1</sup> for the sliding distances s=3 m and s=4.5 m respectively. The measured friction coefficients gave the average value with the standard deviation  $f_{Fr}$ =0.7±0.2 for both load cases.

The contact flash temperatures were analysed according to the method suggested by Archard [8]. The friction heat flux q'' (W/m<sup>2</sup>) considering the uniform heat generation

$$q'' = f_{Fr} p v$$

was assumed to penetrate separately and without division into both contacting bodies. The term p denotes here the average normal contact pressure over the apparent contact area, calculated by neglecting the system deformations as

$$p = \frac{F_{\rm N}}{\pi [R^2 - (R - h)^2]}$$

The average and maximum flash temperatures were calculated for both bodies being heated by a circular uniform heat source, (Fig. 8). The radiation and convection were neglected. The following formulae [9]

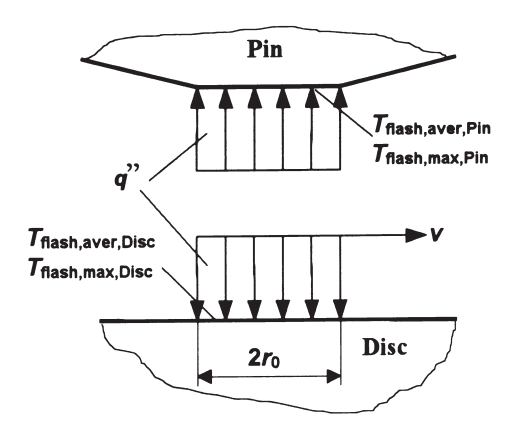


Fig. 8. Heating of bodies with the uniform circular heat source.

$$\begin{cases} T_{\text{flash,aver}} = \frac{1.22r_0q''}{K_{\text{m}}\sqrt{\pi(0.6575 + Pe)}} \\ T_{\text{flash,max}} = \frac{2r_0q''}{K_{\text{m}}\sqrt{\pi(1.273 + Pe)}} \end{cases}$$

were used and the contact flash temperatures were determined by [8]

$$\frac{1}{T_{\rm flash,Contact}} = \frac{1}{T_{\rm flash,Pin}} + \frac{1}{T_{\rm flash,Disc}}$$

The dimensionless parameter  $Pe=0.5\tilde{v}=vr_0/2a_0$  is the Péclet number. The calculated flash temperatures did not exceed the value 6 K [Fig. 6(d)].

The wear test normalised velocities and pressures were  $\tilde{v}$ =0.2, ..., 1.6,  $\tilde{p}$ =0.007, ..., 0.27 and  $\tilde{v}$ =0.3, ..., 2.0,  $\tilde{p}$ =0.009, ..., 0.37 in the cases with normal loads  $F_N$ =21 N and  $F_N$ =50 N, respectively. The higher values of dimensionless pressure correspond to the initial conditions of the contact and are computed on the basis of average Hertz pressures. The wear mechanism could for both load cases be identified as a delamination or adhesive wear, Fig. 1, obeying the linear wear law, Eq. (3).

## 5. Wear simulation results

Assuming the linear wear law, the FEA wear simulation results can be treated on the basis of wear coefficient—sliding distance change equivalence. The wear depth of the given contact geometry with given loading will not change, if the product ks is not changed, regardless of the values of k and s.

# 5.1. Sphere-on-plane sliding contact

The FE wear simulations were run by the approach and model given above, assuming the linear wear law Eq. (3). The dimensional wear coefficients for the wear simulations were evaluated as k=(1.33±0.54)·10<sup>-13</sup> Pa<sup>-1</sup> with both normal loads  $F_N$ =21 N and  $F_N$ =50 N. The maximum allowed wear increment was fixed to  $\Delta h_{\rm lim}$ =0.1  $\mu$ m in both cases. The solution step wear increments were calculated according to Eq. (3), i.e.  $\Delta h$ = $kp\Delta s$ . The disc was assumed to be the harder counterpart as in the experiments and therefore only the pin suffered wear.

The wear coefficient was treated as a constant. The FEA wear simulation curves compared with the experimental data are shown in Fig. 9. The bold lines mark the wear with the average value of k, thinner lines show the influence of its deviation on wear. The surface conditions change continuously during the rubbing, influ-

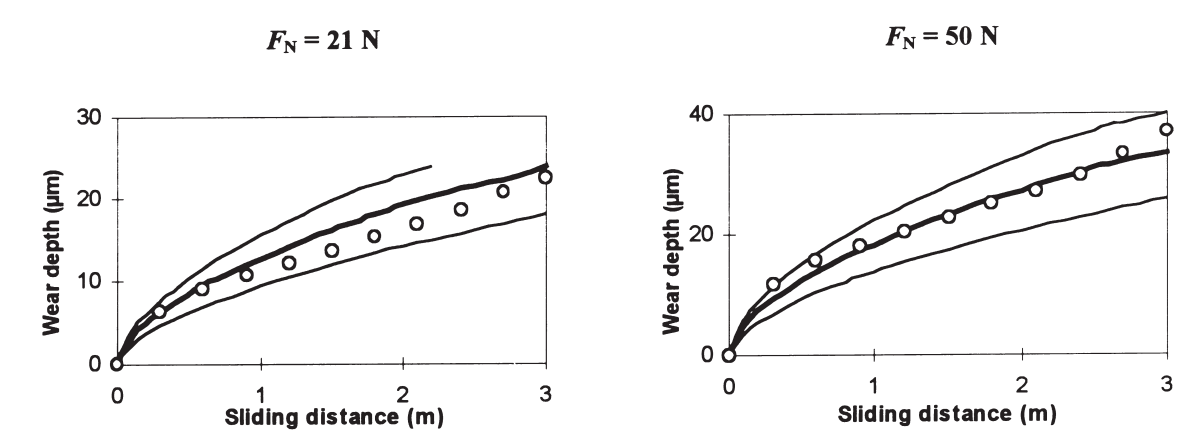


Fig. 9. FEA sphere-on-plane sliding wear simulation results with  $k=(1.33\pm0.54)\cdot10^{-13}$  Pa<sup>-1</sup> (continuous lines, bold one shows the average) compared with experimental data (open circles).

encing the actual wear procedure and the value of the wear coefficient.

# 5.2. Cone-on-cone conforming spinning contact

A cone on a conical socket spinning contact has been analysed [10] with both the cone and the socket being subjected to wear. In the case of the conforming contact the contact area size does not change during the wear procedure and the wear characteristic is nearly linear (Fig. 10). The dimensional wear coefficient k=(1.33±0.54)·10<sup>-13</sup> Pa<sup>-1</sup> was used for the model, as above. The cone angle was  $\alpha$ =60°, the axial load was  $\beta$ =40 N and the bodies were made of steel.

# 5.3. Cone-on-cone non-conforming spinning contact

In the case of non-conforming conical contact the contact area increases along with the wear procedure. Two different cases of non-conformity were analysed with the angle differences  $\Delta\alpha=10'$  and  $\Delta\alpha=20'$ . The load and

wear coefficient were the same as above with the nominal cone angle  $\alpha$ =60° (Fig. 11).

# 5.4. Cone-on-torus spinning contact

The spinning contact with the same cone as above against the torus-shaped socket with the contact surface radius  $R_1$ =37.5 mm was also analysed with FEM assuming the same materials and loading, Fig. 12.

The shape of the particular wear curve for a given contact geometry and loading is determined by the change of the apparent contact area during the rubbing.

A relevant question is which wear simulation accuracy should be expected. It has been reported that the wear coefficient values differ from test to test at least by about a factor of two [11]. The present pin-on-disc experiments gave the wear coefficient values with the standard deviation of ±41%. It is therefore questionable if the simulation results can be used for prediction of life of a particular contact system. The results can, however, rather be used to compare different design solutions and options instead. The influence of the cone and conical

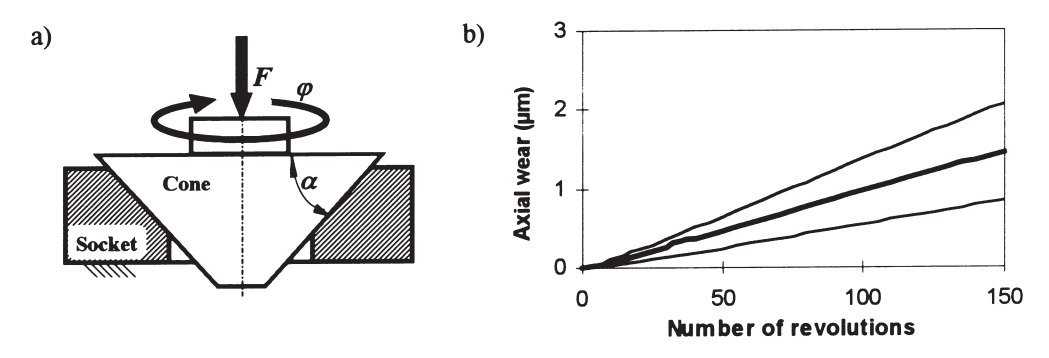


Fig. 10. Wear of conforming conical spinning contact: (a) contact scheme; (b) FEA wear graphs with  $k=(1.33\pm0.54)\cdot10^{-13}$  Pa<sup>-1</sup> (bold line shows the average).

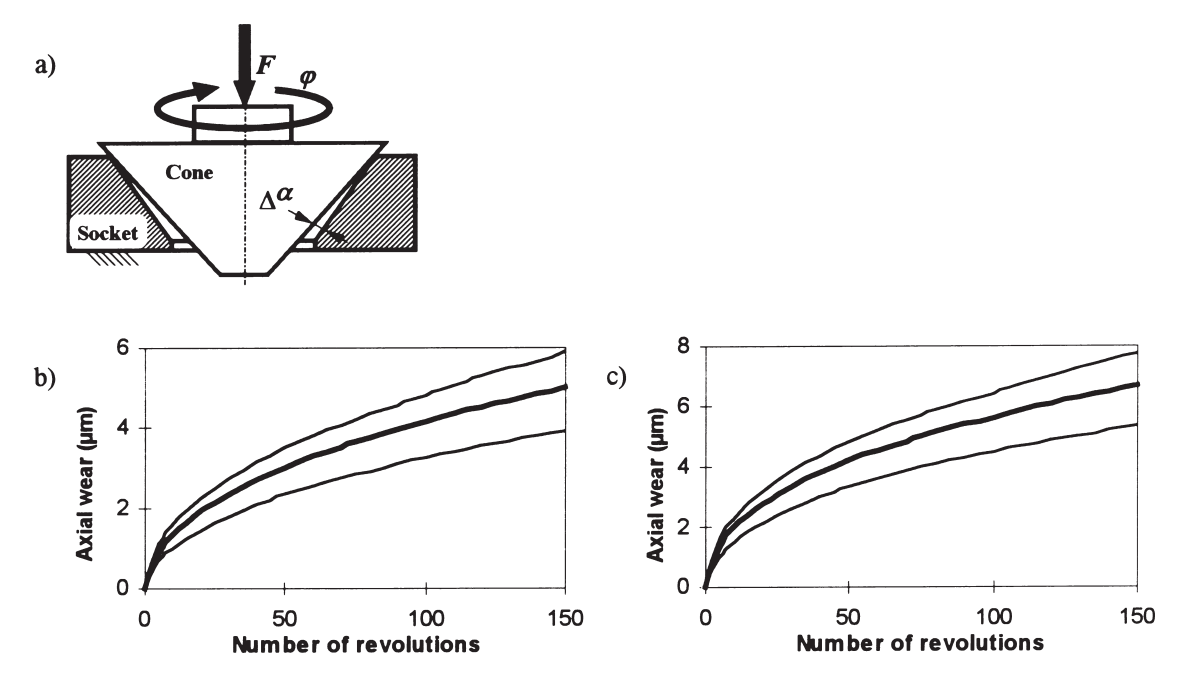


Fig. 11. Wear of non-conforming conical spinning contact: (a) contact scheme; (b) FEA wear graphs with  $\Delta\alpha$ =10'; (c) FEA wear graphs with  $\Delta\alpha$ =20'; k=(1.33±0.54)·10<sup>-13</sup> Pa<sup>-1</sup> (bold lines show the average).

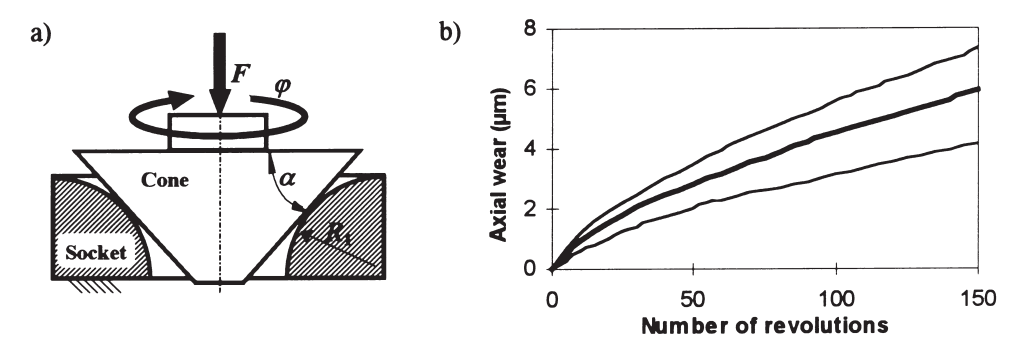


Fig. 12. Wear of cone-on-torus spinning contact: (a) contact scheme; (b) FEA wear graphs with  $k=(1.33\pm0.54)\cdot10^{-13}$  Pa<sup>-1</sup> (bold line shows the average).

socket angle difference  $\Delta\alpha$ =20' on the wear, compared with the conforming conical contact and cone-on-torus contact wear behaviour, considering the wear coefficient standard deviation, is shown in Fig. 13.

# 6. Discussion and conclusions

The FEA numerical solution accuracy depends on the model discretisation. Finer nodal mesh gives more exact results, but contributes to a long computing time and use of greater disk space. Several additional routines are often needed to enhance the numerical procedure and validate the results.

The contact analysis in FEM is a non-linear problem. The FE model discretisation and contact stiffness with given loading and constraints are directly related to the iterative procedure's ability to converge. A good configuration has to be found on the basis of experience.

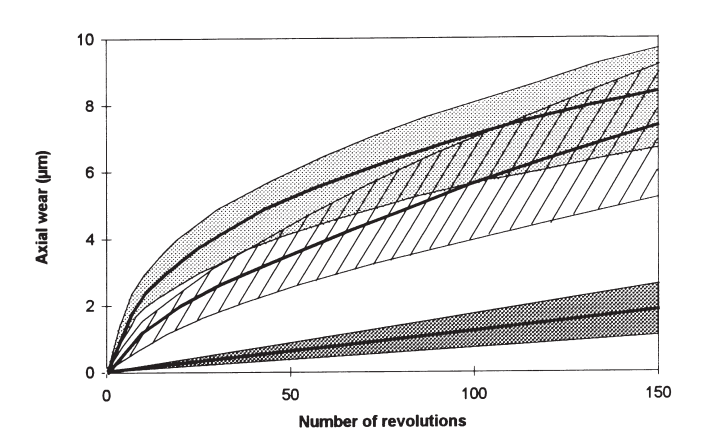


Fig. 13. FEA wear simulation results of the conical spinning contact with different configuration, F=40 N,  $\alpha$ =60°, k=(1.33 $\pm$ 0.54) $\cdot$ 10<sup>-13</sup> Pa<sup>-1</sup> (bold lines show the average): cone-on-cone conforming (dark grey pattern); cone-on-cone non-conforming with  $\Delta\alpha$ =20′ (light grey pattern); cone-on-torus,  $R_1$ =37.5 mm (dashed pattern).

The integration time step is a critical parameter regarding the reliability of simulation results. Too long steps cause erratic results and possibly the un-convergence of FEA procedure. Too short intervals take too much computing time. A simple simulation time step optimisation routine was developed, evaluating the integration step duration for every solution step individually on the basis of the fixed maximum wear increment.

The wear mechanism must be considered and its changes must be foreseen during the simulation process. The Lim and Ashby wear map can be used for steels.

Assuming the linear wear law to be valid, the FEA wear simulation results for a given contact geometry and a given load can be treated on the basis of wear coefficient—sliding distance change equivalence.

Due to the model simplifications and the real deviation of input data, the FEA wear simulation results should be evaluated on a relative scale to compare different design options, rather than to be used to predict the absolute wear life.

#### References

 Meng H-C. Wear modelling: Evaluation and categorisation of wear models. Dissertation, University of Michigan, 1994.

- [2] Lim SC, Ashby MF. Wear mechanism maps. Acta metall 1987;35(1):1–24.
- [3] Holm R. Electric contacts. Uppsala: Almqvist and Wiksells Boktryckeri AB, 1946.
- [4] Archard JF. Wear theory and mechanisms. In: Peterson MB, Winer WO, editors. Wear control handbook. New York: ASME, 1980.
- [5] Cook RD. Concepts and applications of finite element analysis. New York: John Wiley and Sons, 1981.
- [6] ANSYS User's manual for revision 5.0, vol. 4, theory. Houston Swanson Analysis System Inc., 1994.
- [7] Spiegel MR. Mathematical handbook of formulas and tables. New York: McGraw-Hill Book Company, 1990.
- [8] Archard JF. The temperature of rubbing surfaces. Wear 1959:2:438-45
- [9] Tian X, Kennedy FE. Maximum and average flash temperatures in sliding contacts. Transactions of the ASME, Journal of Tribology 1994:116:000–0.
- [10] Põdra P. FEA wear simulation of a conical spinning contact. Presented at OST-97 Symposium on Machine Design, 22-23 May 1997, Tallinn (Estonia).
- [11] Rabinowicz E. Wear coefficients—metals. In: Peterson MB, Winer WO, editors. Wear control handbook. New York: ASME, 1980.